CONF-800213-2

BNL-28160
OG 553
CERN/EP-80-35

3/25/80

MASTER

Accurate Computer Simulation of a Drift Chamber

T.J. Killian - BNL

To be submitted to the Proceedings of the 1980 Vienna Wire Chamber Conference

Vienna, Austria

February 27-29, 1980

DISCLAIMER

This book was prepared as an account of work sponsored by an agency of the United States Government. Neither the United States Government nor any agency thereof, nor any of their employees, makes any warranty, express or implied, or assumes any legal liability or responsibility for the accuracy, completeness, or usefulness of any information, apparatus, product, or process disclosed, or represents that its use would not infringe privately owned rights. Reference herein to any specific commercial product, process, or service by trade name, trademark, manufacturer, or otherwise, does not necessarily constitute or imply its endorsement, recommendation, or favoring by the United States Government or any agency thereof. The views and opinions of authors expressed herein do not necessarily state or reflect those of the United States Government or any agency thereof.

The submitted manuscript has been authored under contract DE-AC02-76CH00016 with the U.S. Department of Energy. Accordingly, the U.S. Government retains a nonexclusive, royalty-free license to publish or reproduce the published form of this contribution, or allow others to do so, for U.S. Government purposes.

DISTRIBUTION OF THIS DOCUMENT IS UNLIMITED

CERN/EP-80-35
25.3.1980

EUROPEAN ORGANIZATION FOR NUCLEAR RESEARCH *

ACCURATE COMPUTER SIMULATION OF A DRIFT CHAMBER

T.J. KILLIAN - BNL

We describe a general purpose program for drift chamber studies. First the capacitance matrix is calculated using a Green's function technique. The matrix is used in a linear-least-squares fit to choose optimal operating voltages. Next the electric field is computed, and given knowledge of gas parameters and magnetic field environment, a family of election trajectories is determined. These are finally used to make drift distance vs time curves which may be used directly by a track reconstruction program. We compare results with data obtained from the cylindrical chamber in the Axial Field Manget experiment at the CERN ISR.

To be submitted to the Proceedings of the 1980 Vienna Wire Chamber Conference

*Research carried out under the auspices of the United States Department of Energy under Contract No. DE-AC02-76CH00016.
TJK/mm

The drift chamber in the Axial Field Magnet experiment at the CERN ISR is used for momentum reconstruction in a 0.5 T magnetic field and for particle identification via dE/dx. To accomplish the former, one requires an accurate distance vs drift time function, while the latter is facilitated by having the same gas gain on all sense wires. The goals of the simulation described here are thus two-fold: first, to calculate the electrostatic configuration and ensure that the drift field in as uniform as possible and the charges on the sense wires are as close to each other as possible; and secondly, to calculate the corresponding distance vs time function.

The AFS chamber is shown in Fig. 1. It is composed of two semi-cylindrical halves, each of which is made up of three electrically separate "crowns". There are 82 active "sectors", each subtending 4° in azimuth. The sense wires are staggered $\pm.4$ mm with respect to the nominal radial sense plane; spacing between sense wires is 8 mm. There are 42 active sense wires in each sector, giving a total of 3444 wires in the system.

Note that in a crude local approximation, the 4° divergence of the sectors can be neglected. This "square cell" model is useful in getting a feel for chamber behaviour, as we shall see.

FIELD CALCULATION

We first of all assume that the chamber is infinitely long, so that we are dealing with a two-dimensional problem. This allows us to use complex potential theory. Next, we assume that the wire diameter is small compared to the spacing, so that the wires can be treated as line charges. (In the AFS, the conditions are well satisfied: length is 1.4 m, spacing is 4 mm, wire diameters range from 30 to 100 μm). Then we have:

$$\phi(\vec{r}) = P(\vec{r}) + \sum_{k=1}^{n} \lambda_k \, G\,(\vec{r}_k; \vec{r}) \qquad (1)$$

where

$\phi(\vec{r})$ = potential at the point $\vec{r} = (x,y)$

$P(\vec{r})$ = polynomial in x and y to fix up boundary planes, etc.

n = total number of wires in the problem

$\vec{r}_k$ = position of wire number k.

λ_k = charge/unit length on wire k.

$G(\vec{r}_k;\vec{r})$ = potential at $\vec{r}$ due to the presence of a unit charge at $\vec{r}_k$ (the Green's function).

Since the problem is two-dimensional, we have also (setting $z = x + iy$, $z_k = x_k + iy_k$)

$$G(\vec{r}_k\,;\,\vec{r}) = -\frac{1}{2\pi\epsilon_o}\,\mathrm{Re}\,\ln g\,(z_k;\,z) \tag{2}$$

where g has a simple zero at $z = z_k$. The electric field due to (2) is given by the simple expression

$$E_x + iE_y = \frac{1}{2\pi\epsilon_o}\left[\frac{\dot{g}}{g'}\right]^* \tag{3}$$

From a practical computing standpoint, it seems useful to employ complex arithmetic in the evaluation of (3), while for (2) one should resort first to algebra. The reason is that g may grow exponentially in some direction; this possibility should be taken care of by hand. Some examples of g are shown in Fig. 2. The consistency of the program is easily checked by setting up a problem with a large array of wires described by a simple g, and comparing with the result obtained from a single term of the correspondingly more complicated g. For example several rows of wires at the same voltage should look like an infinite lattice.

The heart of the problem is of course to calculate λ_k. Let the voltage applied to the ith wire by V_i; then clearly:

$$V_i = P(\vec{r}_i) + \sum_{k=1}^{n} \lambda_k\, G\,(\vec{r}_k\,;\,\vec{r}_i) \tag{4}$$

In the absence of ground planes, we must also impose

$$\sum_{k=1}^{n} \lambda_k = 0 \tag{5}$$

The diagonal term in (4) must be handled with some care:

$$G(\vec{r}_k;\,\vec{r}_k) \equiv -\frac{1}{2\pi\epsilon_o}\,\mathrm{Re}\,\ln\left[\frac{d}{dz}\,g\,(z_k;\,z)\Big|_{z\,=\,z_k}\rho_k\right] \tag{6}$$

Here ρ_k is the wire radius, assumed to be small enough that the azimuthal dependence of G around the wire can be neglected.

It is convenient to re-write (4) in matrix form:

$$\text{or} \qquad \vec{V} = C^{-1}\,\vec{\lambda} \tag{7}$$

$$\vec{\lambda} = C\,\vec{V} \tag{8}$$

The capacitance matrix C may become quite large (107 x 107 in the AFS middle crown), but it is easy to see on physical grounds that it is quite well conditioned, and if pivotal element methods are used it is not difficult to compute. It may be inconvenient to use in its present form, however, as one does not always vary all the wire voltages independently. It is useful to perform a contraction on C, so that it has one column for each independent voltage parameter.

APPLICATIONS

We will analyze the AFS chamber in the square cell approximation (see Fig. 3). Three quantities are of interest: the average drift field, the field at the sense wire (~ 1n gain), the the electron loss to the potential wires. To get the average drift field, consider the lattice of points in Fig. 3. The potential at such a point $\vec{p}_\ell$ is, from (1) and (8),

$$\phi\,(\vec{p}_\ell) = P\,(\vec{p}_\ell) + \sum_{k=1}^{n} [C\vec{V}]_k \;\; G\,(\vec{r}_k\,;\,\vec{p}_\ell) \tag{9}$$

We define the average drift field E by minimizing

$$\chi_E^2 = \sum_\ell \{\, \phi\,(\vec{p}_\ell) - \phi_o - Ey_\ell \,\}^2 \tag{10}$$

with respect to ϕ_o and E. Since (9) is a linear function of the applied voltage V_D and V_p, (10) is a standard linear - least - squares problem with a solution of the form

$$\begin{pmatrix} \phi_o \\ E \end{pmatrix} = H \begin{pmatrix} V_D \\ V_p \end{pmatrix} \tag{11}$$

Next, to get the field at the sense wire, we simply take the appropriate element of $C\vec{V}$, and divide by the wire radius.

Finally we find the electron loss by noting that this is simply the fraction of field lines which leave the drift wires, but terminate on potential wires instead of sense wires. This fraction is the ratio of the fields:

$$f = \min \left\{ o, \frac{\lambda_p/\rho_p}{\lambda_D/\rho_D} \right\} \qquad (12)$$

f is the ratio of two elements of $\vec{CV}$.

All this information is summarized in the contour plot in Fig. 4. The lines of constant drift field, constant gain, and constant electron loss provide a concise picture of chamber operation under a wide range of operating conditions.

A similar approach is used to handle the actual AFS cylindrical geometry. Here we must allow a different drift voltage for each cell, as well as special voltages on the inner and outer boundary wires (see Fig. 1). Since we want each sense wire to have the same gain, we re-write (10) as

$$\chi^2 = \chi_E^2 + w \sum_{\substack{\text{sense} \\ \text{wires}}} (\lambda_k - \lambda_o)^2 \qquad (13)$$

adding terms in the sense wire charges. For simplicity, we restrict ourselves to a linear range in V_D, constant V_p, and two or three parameters referring to the boundary wires. We then choose E and λ_o, and minimize (13) with respect to

$$\{ V_D, \; V_D, V_p, V_B^{[1]}, \ldots, V_B^{[m]} \} \qquad (14)$$

The results of a gain study are shown in Fig. 5. The data in the upper graph were taken in a test beam at the CERN PS. The high voltage distribution was chosen by studying a number of plots like Fig. 4 for different cell sizes, without worrying about end effects. One notes problems here, in the middle and outer crowns especially. There is also an odd-even variation in gain depending on whether the beam was above or below the sense plane; the effect is that wires staggered closer to the beam have a larger pulse height. We shall have more to say about this later. The lower graph shows data taken at the ISR with the final, optimized, high voltage distribution. The end effects have been eliminated.

DRIFT TIME CALCULATIONS

We take the drift velocity as a given function of the electric and magnetic fields; the electric field is obtained from (3). The path followed

by any electron cloud is then given by integrading a first-order differential equation. The drift time of an assumed particle track is then found as follows:

(1) a family of electron drift paths is computed for the all of interest. This is done using a quartic spline parametrization in an algorithm which is basically the inverse of the one described by Wind[1]. Wind keeps the tracks coordinates fixed and varies the initial position and slopes, while for our purposes we fix the initial conditions and allow the track to move about as it likes. Such drift paths are shown in Figs. 6 and 7;

(2) we find the intersections of the particle track with the drift paths, and determine the time for each (see figs. 8 and 9);

(3) the smallest arrival time is found by interpolating through the points found in step (2).

Final results for tracks of incident at different angles to the sense plane are shown in Figs. 10 and 11. In each case, the dominant linear term has been removed, and what is plotted is the correction to d = vt. These curges agree in shape with those inferred from reconstructed tracks, but the magnitude of the velocity disagrees by 2 to 3%. We are presently putting these revised velocities back into the program, so as to produce new curves which should better reconstruct the data.

REFERENCE

[1] H. Wind, Momentum analysis by using a quintic spline model for the tracks, Nucl. Instr. and Meth. 115 (1974) 431.

FIGURE CAPTIONS

1) Layout of the AFS drift chambers.

2) Examples of Green's functions.

3) Square cell with lattice of test points.

4) Contours in the V_D/V_p plane:
   - solid line: drift field, spacing 0.2 KV/cm
   - dashed line: field at surface of sense wire, spacing 20 KV/cm
   - dotted line: electron loss, spacing 10%.

5) Pulse heights before and after H.V. optimization.

6) Drift paths in the absence of magnetic field.

7) Drift paths in a magnetic field of 0.5 T. The turn angle is 14^o appropriate for 50% argon - 50% ethane.

8) Arrival times corresponding to the paths in Fig. 6.

9) Arrival times corresponding to the paths in Fig. 7.

10) Residual drift time vs distance curves, no magnetic field. Symbols 0, 1, 2, 3, 4 are for track incidence angles of 0^o, 5^o, 10^o, 15^o, 20^o, respectively.

11) Residual drift time vs distance curves in magnetic field of 0.5 T. Symbols as in Fig. 10.

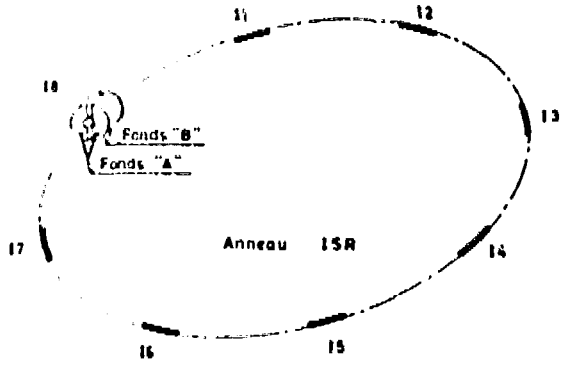

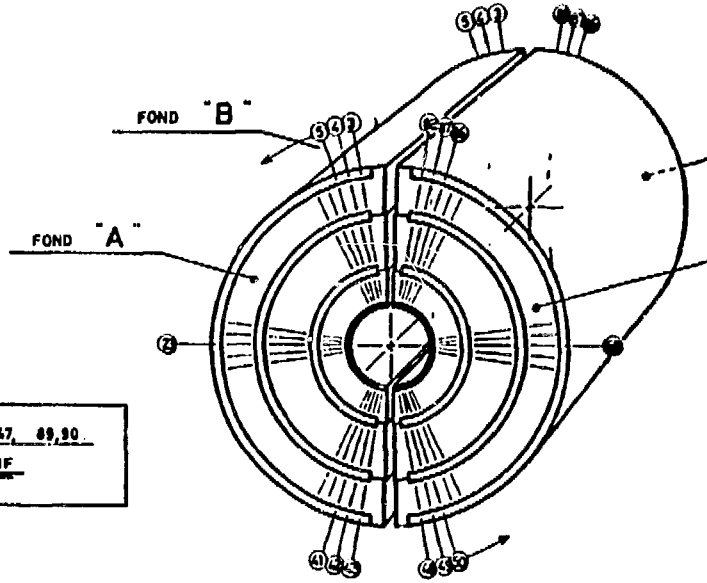

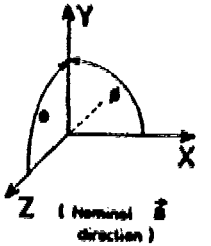

Secteurs : 1, 2, 44, 45, 46, 47, 89, 90.
NON ACTIF

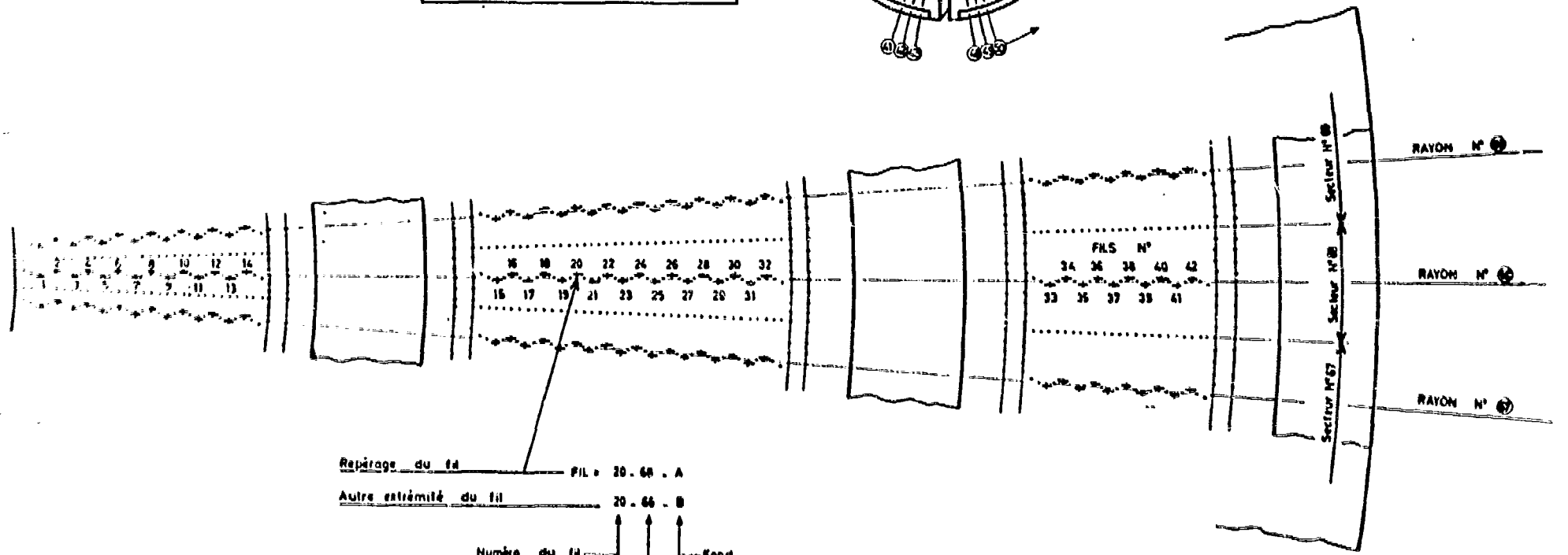

R 807 — Drift Chambers				
Repérage des fils	CERN	EF.264/02_047/3	A	

Examples of $g(z_k ; z)$

1) Single wire — $z - z_k$

2) Row of wires — $\sin \frac{\pi}{s}(z - z_k)$

3) Wire above ground plane — $\frac{z - z_k}{z - z_k + 2id}$

4) Row of wires above ground plane — $\frac{\sin \frac{\pi}{s}(z - z_k)}{\sin \frac{\pi}{s}(z - z_k + 2id)}$

5) Lattice of wires — Weirstrass σ -function with $P(\vec{r}) \sim y^2$

6) Row of wires between two ground planes

7) Wires inside a box

} Superposition of finite number of σ-functions

8) Wires in a ring (AFS geometry) — $z^n - z_k^n$, where $n = \frac{2\pi}{\Delta\phi}$ = integer.

Figure 2

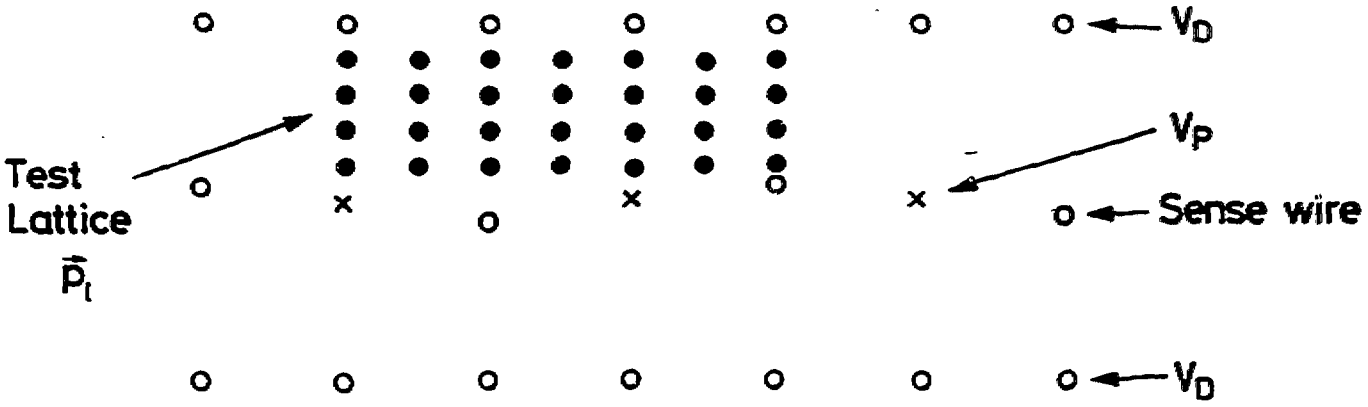

Figure 3

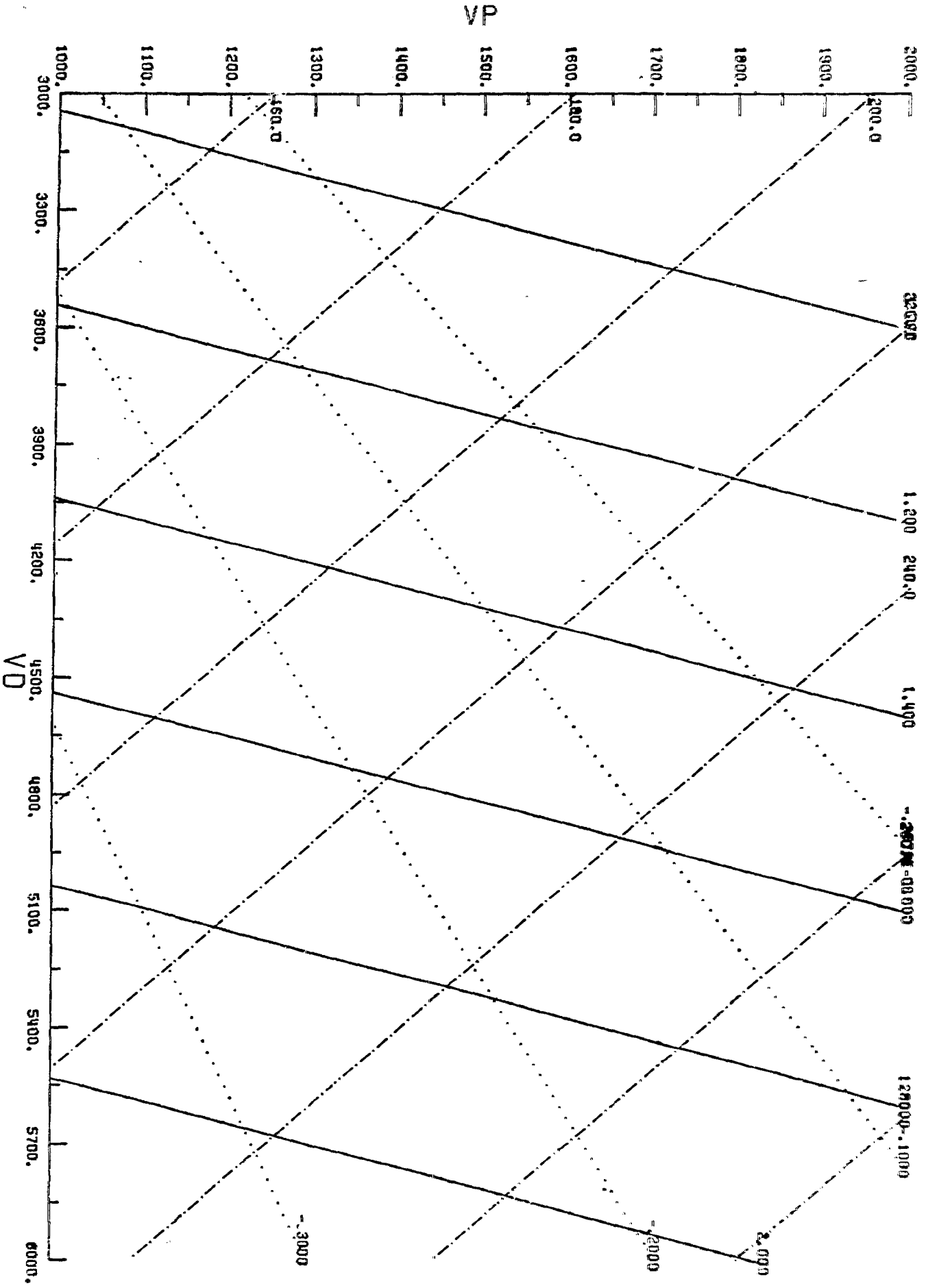
VP
VD
1000.
1100.
1200.
1300.
1400.
1500.
1600.
1700.
1800.
1900.
2000.
3000.
3300.
3600.
3900.
4200.
4500.
4800.
5100.
5400.
5700.
6000.

Figure 4

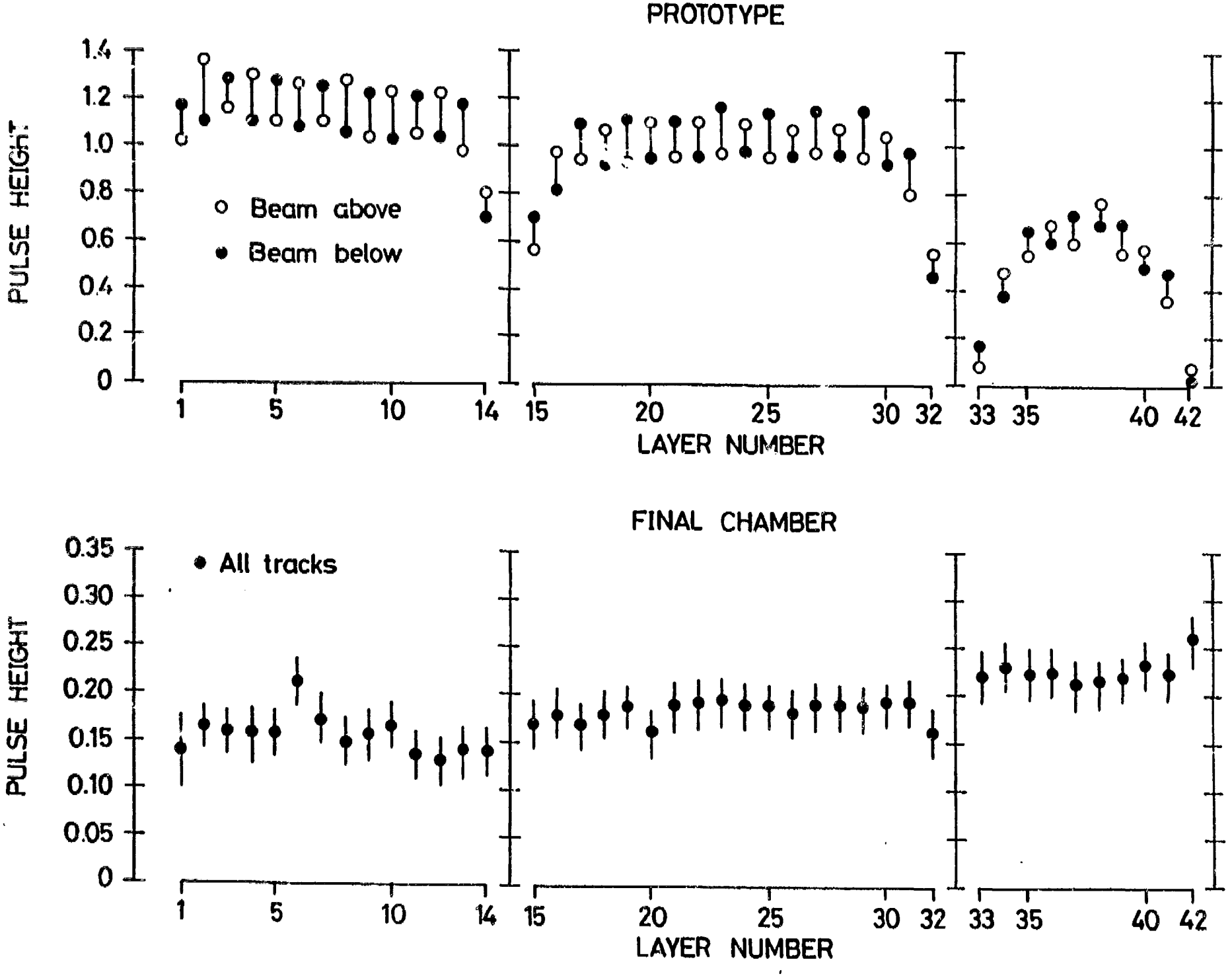
PROTOTYPE
PULSE HEIGHT
1.4
1.2
1.0
0.8
0.6
0.4
0.2
0
Beam above
Beam below
1
5
10
14
15
20
25
30
32
33
35
40
42
LAYER NUMBER
FINAL CHAMBER
PULSE HEIGHT
0.35
0.30
0.25
0.20
0.15
0.10
0.05
0
All tracks
1
5
10
14
15
20
25
30
32
33
35
40
42
LAYER NUMBER

Figure 5

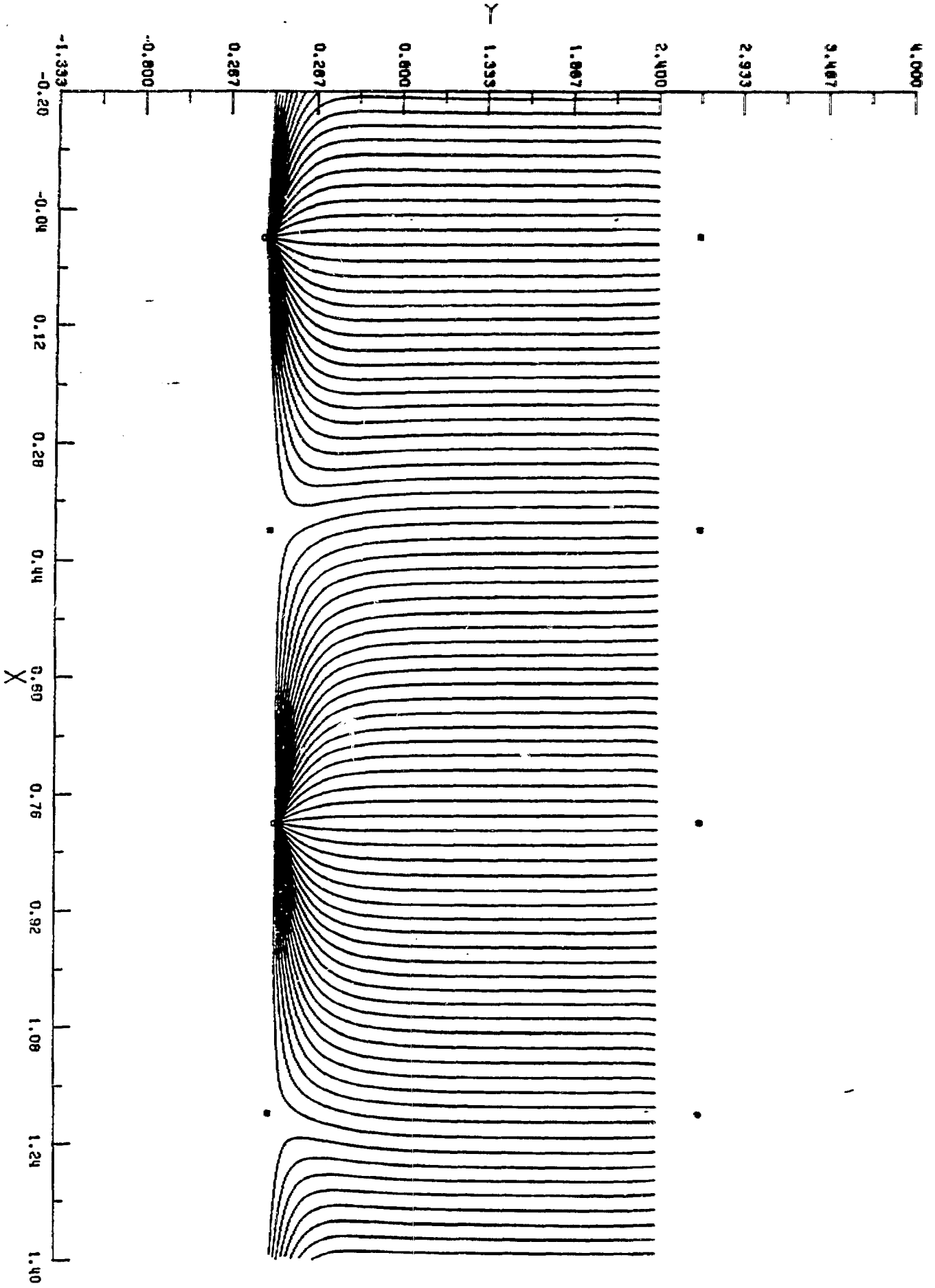
Y
-1.333
-0.800
-0.267
0.267
0.800
1.333
1.867
2.400
2.933
3.467
4.000
X
-0.20
-0.04
0.12
0.28
0.44
0.60
0.76
0.92
1.08
1.24
1.40

Figure 6

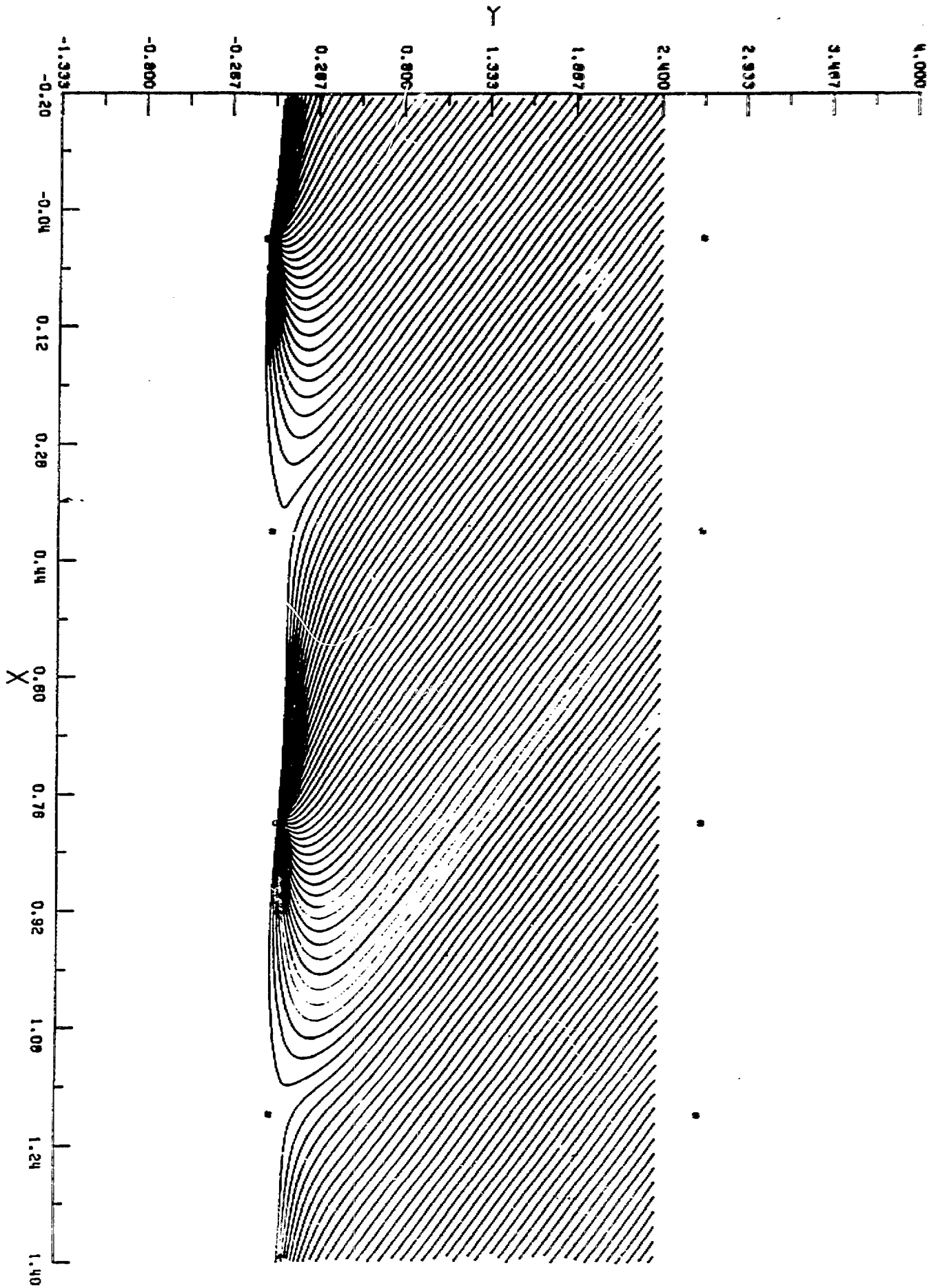
Y
-1.333
-0.800
-0.267
0.267
0.800
1.333
1.867
2.400
2.933
3.467
4.000
X
-0.20
-0.04
0.12
0.28
0.44
0.60
0.76
0.92
1.08
1.24
1.40

Figure 7

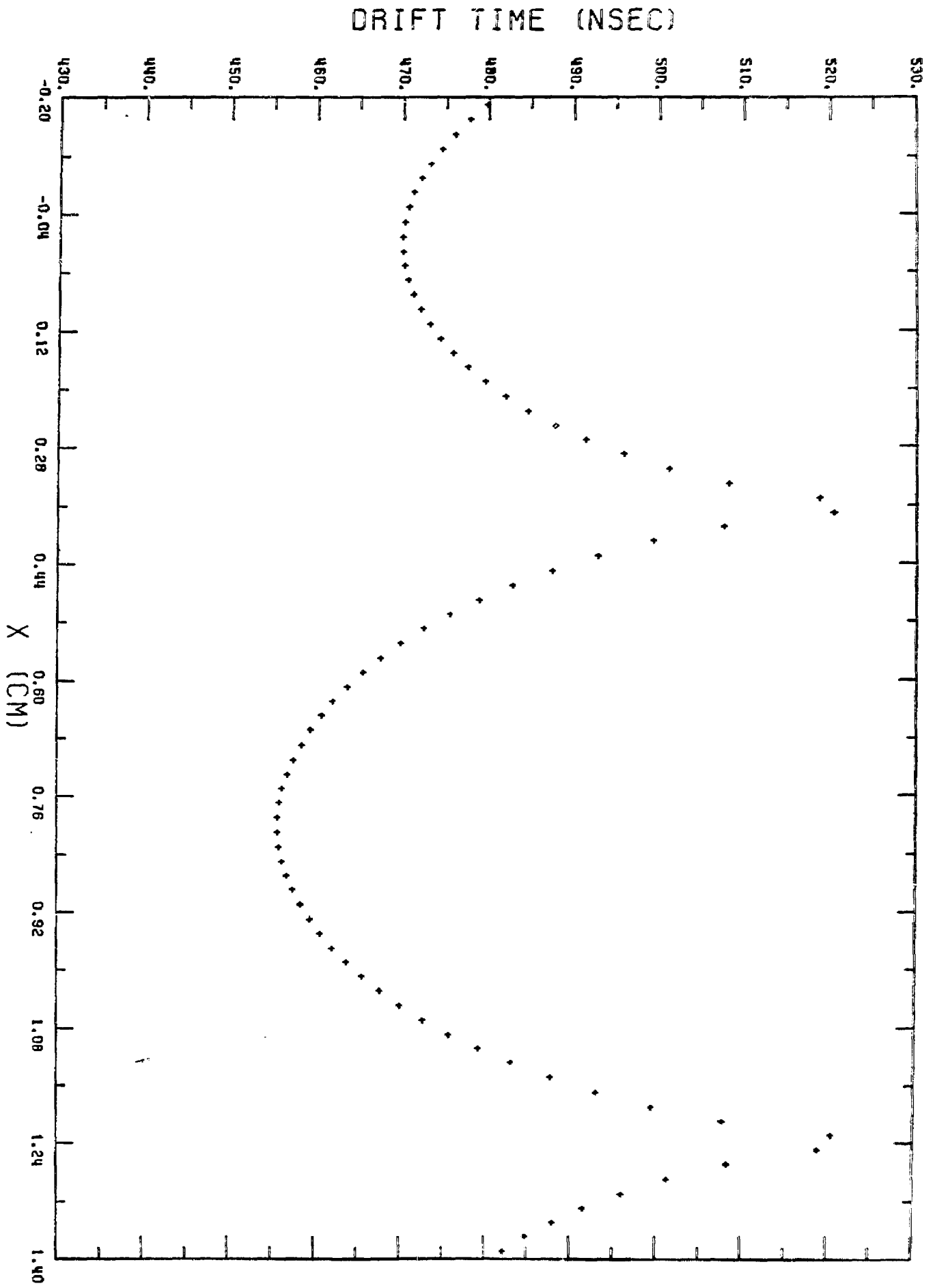
DRIFT TIME (NSEC)
430.
440.
450.
460.
470.
480.
490.
500.
510.
520.
530.
-0.20
-0.04
0.12
0.28
0.44
0.60
0.76
0.92
1.08
1.24
1.40
X (CM)

Figure 8

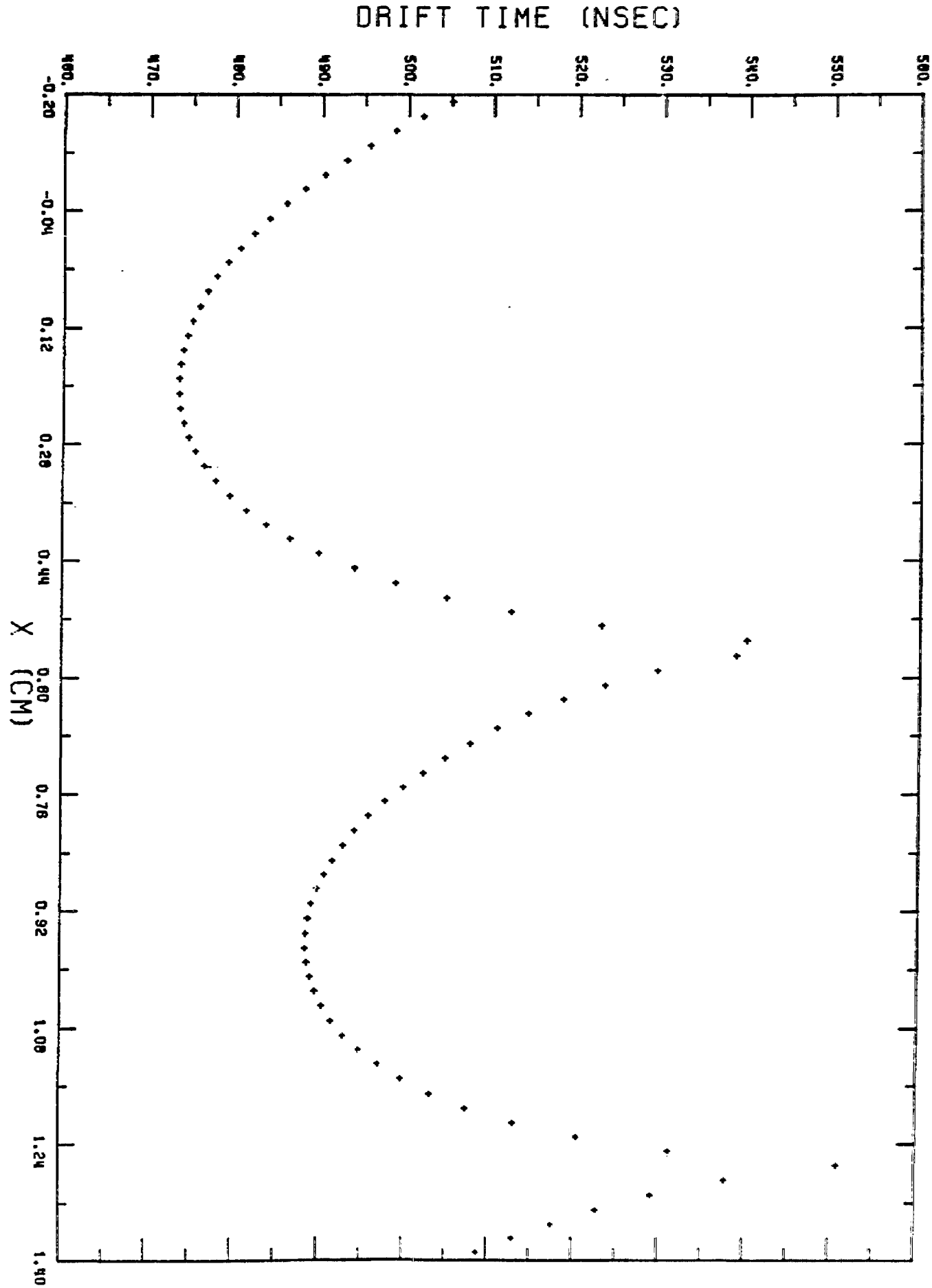
DRIFT TIME (NSEC)
460.
470.
480.
490.
500.
510.
520.
530.
540.
550.
560.
-0.20
-0.04
0.12
0.28
0.44
0.60
0.76
0.92
1.08
1.24
1.40
X (CM)

Figure 9

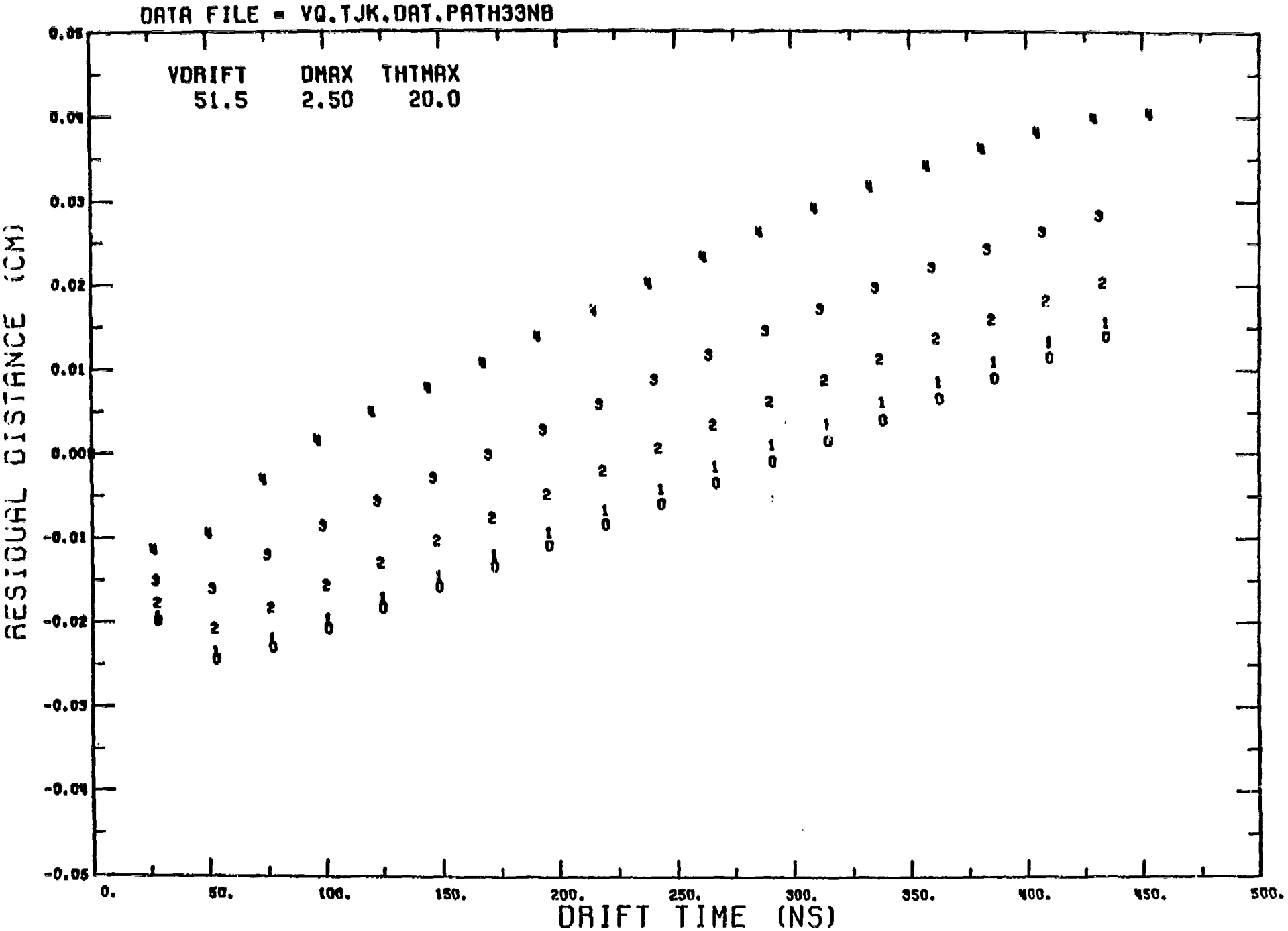
DATA FILE = VQ.TJK.DAT.PATH33NB
VDRIFT DMAX THTMAX
51.5 2.50 20.0
RESIDUAL DISTANCE (CM)
DRIFT TIME (NS)
0.05
0.04
0.03
0.02
0.01
0.00
-0.01
-0.02
-0.03
-0.04
-0.05
0.
50.
100.
150.
200.
250.
300.
350.
400.
450.
500.

Figure 10

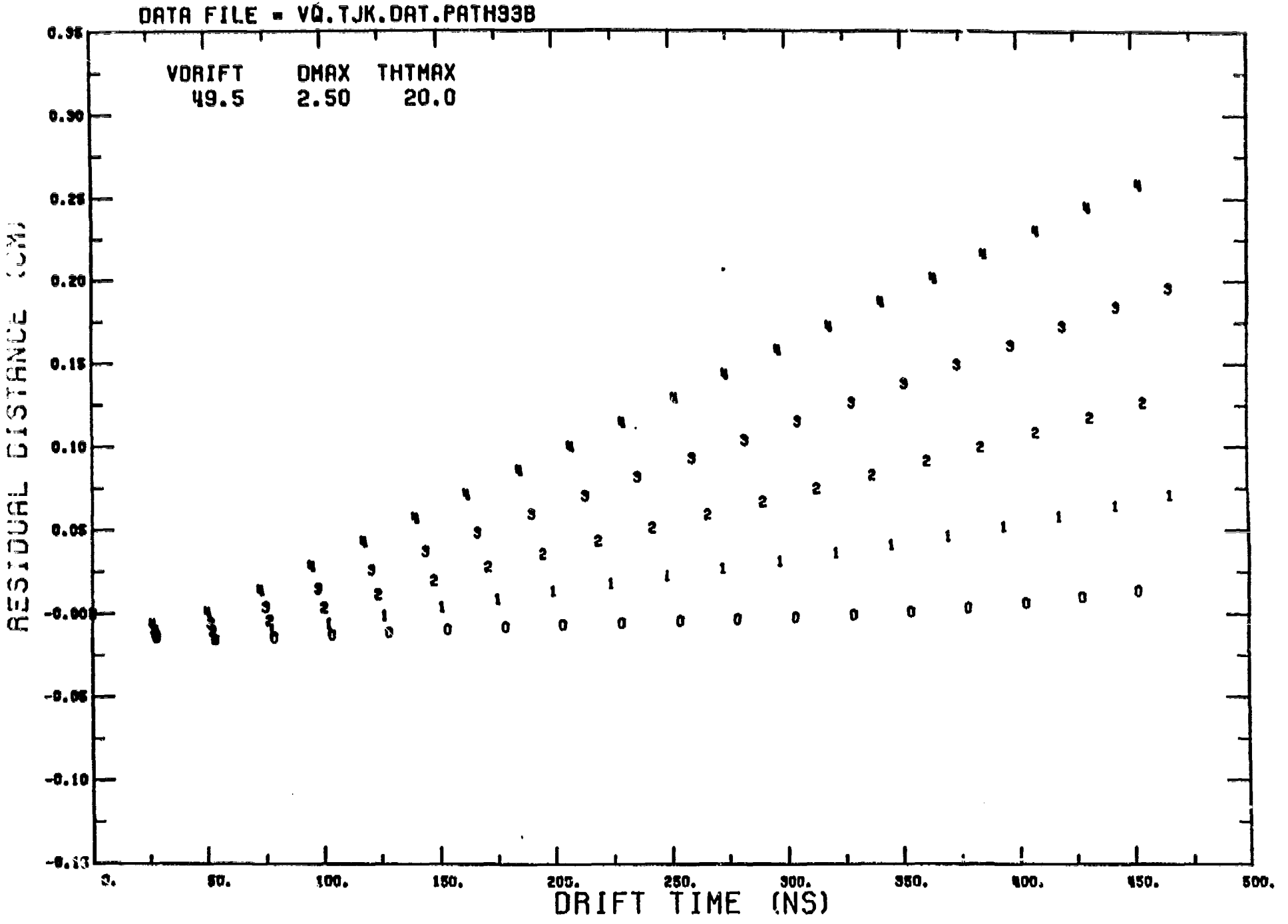
DATA FILE = VQ.TJK.DAT.PATH93B
VDRIFT 49.5
DMAX 2.50
THTMAX 20.0
RESIDUAL DISTANCE (CM)
DRIFT TIME (NS)
0.30
0.25
0.20
0.15
0.10
0.05
-0.00
-0.05
-0.10
-0.13
0.
50.
100.
150.
200.
250.
300.
350.
400.
450.
500.

Figure 11